

A V-Band Survey for Variable Galactic Nuclei in the Hubble Deep Field

Vicki L. Sarajedini

University of Florida, Gainesville, FL 32611

`vicki@astro.ufl.edu`

Ronald L. Gilliland

Space Telescope Science Institute, 3700 San Martin Drive, Baltimore, MD 21218

`gillil@stsci.edu`

and

Christina Kasm

University of Florida, Gainesville, FL 32611

`ckasm@astro.ufl.edu`

ABSTRACT

We present the results of a 2-epoch variability survey in the Hubble Deep Field with the goal of investigating the population of AGN to $z \simeq 1$. The high resolution and stability of HST allows accurate photometry to be obtained within subarcsecond apertures, resulting in the ability to probe much lower AGN/host galaxy luminosity ratios than can be done from the ground. The primary data sets analyzed for galactic variability are the original HDF observations obtained in December 1995 and a second V-band (F606W) image obtained almost exactly 5 years later in 2000. We find evidence for nuclear variability in 16 of 217 galaxies brighter than $V_{nuc} = 27.5$. Correcting for incompleteness and spurious detections, variable nuclei make up $\sim 8\%$ of the surveyed galaxies. These sources have a redshift range of $0.09 < z < 1.8$ and cover the full range of galaxy nuclear V–I colors. Seven of our variable sources are coincident with X-ray sources detected in the 2Ms Chandra survey; six from the main catalog and one from the supplementary catalog. We find that 44% of the variable nuclei are associated with mid-IR detections at $15\mu\text{m}$ and 31% are detected at 1.4GHz. Optical spectra are available for 13 of the 16 variables. One is a broad-line AGN and 2 others show weak

evidence of type 2 AGNs. With the assumption that these variables are all active nuclei, we estimate the AGN LF at $0.4 < z < 1.1$ extending to $M_B \simeq -15$. We find evidence for an increase in the number density of faint AGN when comparing to the local Seyfert luminosity function. The LF for optically varying nuclei appears to rise in number density with no evidence of turning over at these faint magnitudes.

Subject headings: galaxies:active–surveys

1. INTRODUCTION

An important goal of modern cosmology is to understand the evolution of active galaxies and their relationship to normal galaxy evolution. A key piece of information needed to further this understanding is an accurate knowledge of the luminosity function (LF) for AGN over a wide range of absolute magnitudes and redshifts. The AGN LF is populated by quasars at the bright end (e.g. Hartwick & Schade 1990) and Seyfert galaxy nuclei, considered to be their intrinsically fainter counterparts, at the low luminosity end (Cheng *et al.* 1985; Huchra & Burg 1992; Maiolino & Rieke 1995; Koehler *et al.* 1997; Ulvestad & Ho 2001; Londish *et al.* 2002).

Understanding how the faint end of the AGN LF evolves is of particular importance for determining the frequency and total space density of AGNs at earlier epochs. This has obvious implications for determining their total contribution to the X-ray, IR and UV backgrounds. Large numbers of low-luminosity AGN have been proposed to explain the ionization of the intergalactic medium at high redshift (Steidel & Sargent 1989), although recent observational and theoretical results differ on the amount of their true contribution (Barger 2003; Schirber & Bullock 2003). Additionally, the faint end is an important constraint on evolutionary models for the AGN LF such as pure luminosity and luminosity-dependent density evolution (e.g. Boyle *et al.* 2000).

One method to identify AGN in imaging surveys is via their variable nature. QSOs and Seyfert galaxies have long been known as variable objects, with significant optical flux changes occurring on timescales of months to several years. Variability has been a successful method for identifying AGNs, primarily QSOs (Hawkins 1986; Koo *et al.* 1986; Hook *et al.* 1994). A survey for variable sources in SA57 revealed many optically extended, Seyfert-like galaxies (Bershady *et al.* 1998) which generally had higher variability amplitudes than the more luminous QSOs. This result suggests that variability is a good technique for selecting intrinsically faint QSOs and Seyfert nuclei.

While variability and other selection techniques (spectroscopy, color selection, etc.) have been successful in finding QSOs out to high redshifts, the intrinsically fainter AGN (i.e. Seyfert galaxies) have been difficult to detect beyond the local universe. Ground-based variability surveys, like spectroscopic surveys, are quickly limited to AGN which dominate the host galaxy light at higher redshift. Recent X-ray surveys with Chandra and XMM-Newton have revealed hundreds of X-ray sources at $z \simeq 1$. Many of these are confirmed AGN but still many more are ambiguous in nature (e.g Barger *et al.* 2002). In summary, the population of moderate-to-high redshift, low-luminosity AGN has not been well surveyed and the evolution of the faint end of the AGN LF is still poorly known.

In this study, we have searched for optical nuclear variability in HDF¹ galaxies to identify the population of active galaxies out to $z \sim 1$. The primary data sets analyzed for galactic variability are the original HDF observations (Williams *et al.* 1996) obtained in December 1995 and a second V-band (F606W) image obtained almost exactly 5 years later in December of 2000. The main advantage of HST over ground-based surveys is the ability to do accurate photometry within smaller apertures than can be done from the ground thus allowing us to probe much lower AGN/host galaxy luminosity ratios.

We discuss the details of the image processing and photometry in Section 2, followed by a discussion of the selected varying galactic nuclei in Sections 3 and 4. In Section 5, we cross-reference our sources with various multi-wavelength surveys. A discussion of the optical spectra for the varying sources is presented in Section 6. In Section 7, we present the luminosity function for variable nuclei. We close with a summary of our conclusions in Section 8.

2. PHOTOMETRY

2.1. Image Processing

The original epoch HDF data in F606W consisted of 108 individual exposures with a total integration time of 113,050 seconds. These data were obtained with a total of 9 unique dithers covering both sub-pixel offsets and multiple pixels on a scale of about ± 10 WF pixels. The primary data processing technique was detailed in Gilliland, Nugent, and Phillips (1999) for creation of over-sampled, by a factor of four, summed images with resulting noise and resolution properties competitive with, and sometimes slightly better than those reported in Williams *et al.* (1996). The mean epoch of the original F606W data was MJD 50076.9.

¹HDF refers to the Hubble Deep Field North

Exposure times used for the original epoch ranged from 350 to 1500 seconds with a mean sky rate of 0.0758 e-/s.

The second epoch HDF data in F606W was taken with GO-8389 (PI Rodrigo Ibata) with a science goal distinct from that here, but one that also required precise differential measurements across the two epochs. These data consisted of 70 individual exposures each of 1300 seconds for a total exposure time of 91,000 seconds. The goal was to have the new data obtained at the same pointing as the original HDF, and at the same orientation, and with dithering over the same spatial scale, but with an improved level of sampling using 35 unique dithers. This goal was quite well met, thus resulting in quite similar data in the two F606W epochs. The mean epoch of the second F606W data was MJD 51882.9 implying a delta of 4.94 years. The mean sky rate for the newer epoch was 0.0958 e-/s. Processing of the second epoch data was identical to that of the first, using the same software as described in Gilliland, Nugent and Phillips (1999). To facilitate simple, robust analysis of data from the two epochs the registrations of the second epoch were evaluated using a grid of galaxies from the original epoch (stars could not be used since these show unique proper motions over five years); this results in second epoch over-sampled combined images that are accurately aligned to the first epoch with *maximum* errors of ~ 0.05 pixels. Therefore, comparative analysis for change across epochs can be made using precisely the same pixels, mapping back to common physical domains. For both epochs, each individual frame was sky subtracted before combining, cosmic rays were eliminated (affected pixels assigned zero weight in the combination) and hot pixels subtracted.

The extreme stability provided by *HST* is an essential factor in being able to probe to unique sensitivity levels with these extensive observations. Limiting factors, to be discussed further below, arise from (1) a time-varying Charge Transfer Efficiency (CTE) that must be empirically corrected for, and (2) limited sub-pixel dithering in the first HDF epoch that results in minor mismatches noticeable for the objects with tight cores at high signal to noise.

2.2. Source Selection and Aperture Size

We created a catalog of HDF objects using DAOFIND in IRAF² to ensure a systematic selection of all sources in the V-band images. All objects above the 8σ detection threshold

²IRAF is distributed by the National Optical Astronomy Observatories, which are operated by the Association of Universities for Research in Astronomy, Inc., under cooperative agreement with the National Science Foundation.

were identified in the 1995 images (the deeper of the two) using a kernel size of $1.8\times$ the semi-major axis of the Gaussian convolution kernel (1.3 pixels) to allow more sensitivity to extended objects. The catalog was then edited to remove a minority of objects that did not appear to be centered on galaxies (i.e. multiple detections within single galaxies). For very amorphous galaxies with no clear center, all bright “knots” appearing within the source were retained in the catalog.

For our photometry, we chose a small aperture consistent with the FWHM of stellar sources in the field. Stars have $\text{FWHM} \simeq 5.5$ pixels in the over-sampled images corresponding to $\sim 0.14''$. We chose an aperture size of 6 pixels in diameter to be most sensitive to photometric changes in an unresolved nucleus. This approach differs from that taken in Sarajedini, Gilliland & Phillips (2000; hereafter SGP), where the aperture size was scaled to the size of the galaxy. Our goal here is to provide better sensitivity to variable active nuclei with less dilution from the underlying, non-varying host galaxy light.

Aperture photometry for all sources was performed on the direct images using the PHOT algorithm in IRAF. Because the second epoch image was aligned with the first, exactly the same pixels were used in both epochs. During image processing, the background was subtracted and the images were scaled to an exposure time of 6000s. This allowed the sky value to be held constant at zero for both epochs and all WF CCDs. The resulting nuclear magnitudes for each galaxy in the HDF were then adjusted by a zero-point offset to bring them into agreement with the integrated, isophotal galaxy V-band AB magnitudes of Williams *et al.* (1996).

2.3. Charge Transfer Efficiency Losses And Photometric Errors

After performing aperture photometry, nuclear variability can then be determined by simply obtaining the difference in magnitude for each source over the two epochs. Figure 1 shows the magnitude difference between the 1995 and 2000 images as a function of magnitude within an aperture of $r=3$ pixels, the equivalent of $0.15''$ in diameter. The solid line represents no difference in magnitude between the two epochs.

The main culprit producing the obvious offset from the solid line is charge transfer efficiency (CTE) losses. As in SGP, we find a clear correlation of the photometric differences with position on the CCD and magnitude. This is the well known CTE effect (Whitmore *et al.* 1999; Biretta *et al.* 2001) which causes targets far from the CCD readout amplifier to appear fainter than similar targets near the amplifier. For this reason, the effect is usually more significant in the Y-direction, (the direction of the readout down the CCD) than the

X-direction (the direction of the readout of the shift register at the bottom of the CCD). Although the 1995–1997 I-band study did not show significant correlations in the X-direction, the longer time interval sampled here does show a significant correlation in the X-direction for all 3 WF CCDs. Additionally, we note that the slope of the relation is generally steeper in the Y-direction than had been determined in SGP. This is expected due to the longer 5 year time interval between epochs in this study.

We first attempted to fit the relationship between object position, magnitude difference and magnitude globally for all 3 WF CCDs as done in SGP. However, we found that this approach was not sufficient to equally remove the CTE effect from all WF CCDs. Differences in the slope of the relation between the CCDs were significant and could easily be determined for each CCD individually. We adopted a two-step approach to determine this relationship. First, we fit a linear surface to the X and Y object positions and the magnitude differences using SURFIT in IRAF for each CCD. While the slope of the fit was found to be significant with both the X and Y positions, the value of the slope was steeper with Y position in all 3 WF CCDs, consistent with what is expected for CTE losses. The slope of the relation between Y position and magnitude difference was found to be -2.6×10^{-5} , -1.3×10^{-5} and -1.46×10^{-5} mag/pixel for WF2, WF3 and WF4 respectively. The slope of the relation with X position, while significant, was found to be about an order of magnitude lower in all 3 WF CCDs. These fits were used to correct the magnitude difference values for position-dependent offsets. Secondly we fit the dependence of the magnitude difference with nuclear magnitude. A 3rd order fit was required to properly model the dependence in all 3 WF CCDs. After applying this correction to the data in Figure 1, the resulting photometric differences are shown in Figure 2 as a function of nuclear magnitude.

Finally, we determine the expected noise level for non-variable sources. As in SGP, we divided the full set of individual exposures into two sets composed simply of the odd-numbered frames and the even-numbered frames. Each set represents an “epoch” without any real time difference. These images effectively carry through the effects of object and sky Poisson noise, readout noise, and possible errors in the adopted sky zero points.

The magnitude of each galaxy was then measured in the odd and even data sets and difference in magnitude vs. the average magnitude within $r=3$ pixel apertures is shown in Figure 3a. Figure 3b is the RMS of the intensity differences shown in a) within unity magnitude intervals. The solid line represents a quadratic fit to the points which is the adopted 1σ galaxy photometric error as a function of magnitude.

The precision of the photometry must be independently limited at the bright end of the distribution, since systematic effects not captured by the odd-even data set comparisons become limiting factors (e.g. the sometimes poor distribution of sub-pixel phase-space dithers

in the first epoch data). In SGP, we adopted a floor of 1.2%. Here we adopt a more conservative value of 1.5% consistent with the use of much smaller apertures on average for bright sources in the current study than in SGP. As should be apparent, this is a reasonable limit for photometric precision to adopt, but in detail remains somewhat arbitrary.

3. SELECTION OF VARIABLES AND SURVEY COMPLETENESS

Figure 4a is the absolute value, CTE-corrected magnitude differences for sources in the HDF. The solid line represents the 3σ limit for variability significance ($3\times$ the RMS indicated by the solid line in Figure 3b). Objects above this limit are selected as significant variables and are indicated with open hexagons. Figure 4b is the result of normalizing the magnitude difference by this solid line. Here the Y-axis indicates the level of significance of each source in units of σ . The X-axis extends at the faint end to $V_{nuc}=29.0$, which is the estimated photometric completeness magnitude limit for galaxy nuclei in this survey. Beyond this limit, the number counts for galaxies in the HDF begin to decrease.

We find sixteen galaxies whose nuclei have undergone at least a 3σ variation over the 5 year time interval. These sources are listed in Table 1 with columns as follows: (1) Williams *et al.* (1996) ID, (2) & (3) RA & DEC (J2000), (4) Redshift from the literature, (5) Spectral type based on photometry from Fernández-Soto, Lanzetta and Yahil (1999, hereafter: FLY), (6) V_{nuc} internal to $r=3$ pixel aperture, (7) Magnitude difference between 1995 and 2000; positive implies brighter in 1995, (8) Significance of change obtained when normalized by the expected error as a function of magnitude, (8) Bulge-to-Total (B/T) 2-dimensional model fits for the I(F814W) images from Marleau & Simard (1998). The last several columns relate to the source detection at other wavelengths discussed in Section 5.

There are two distinct completeness issues that effect our survey. The first is related to the incomplete time-sampling of the variable sources we wish to detect. Most variability surveys employ a method where the survey field is imaged several times over many years (e.g. Trevese *et al.* 1994; Hawkins 2002). Depending on the quality of the data, these surveys have shown that virtually all known AGN will be found to vary if observed periodically over several years. Our study is limited by the fact that we have only two epochs with which to determine variability and therefore sample just two points on the lightcurve of a varying source. Because of this, we will be incomplete in our census of AGN since some varying sources could lie at magnitudes close to their original magnitude measured 5 years earlier and would thus go undetected in our survey.

We estimate our incompleteness due to undersampling of the lightcurve by using variabil-

ity data for AGN obtained over many years. We randomly select points along the lightcurve separated by 5 years, the time interval sampled by our HDF images. Because long term variability surveys for low-luminosity AGN have not yet been published, we have conducted this test with two sets of QSO lightcurve data; a sample of PG quasars from Giveon *et al.* (1999) and a sample of SA57 quasars from Trevese *et al.* (1994). Giveon *et al.* monitored 42 quasars over 7 years with a typical sampling interval of 40 days while Trevese *et al.* monitored 64 over 15 years about once a year. Sampling these lightcurves every 5 years and assuming photometric errors typical of our HDF images, we can estimate the probability that these sources would be detected in our survey. We find that $\sim 75\text{--}80\%$ would be detected as varying by at least 3σ with only 2 observations separated by 5 years. Therefore, the results of our analysis are likely to underrepresent the true number of variable nuclei by $\sim 20\text{--}25\%$.

The second incompleteness issue results from the use of a fixed aperture to detect nuclear variability. We have chosen a small, fixed aperture to minimize dilution of the AGN light from the underlying host galaxy to be more sensitive to AGN varying within bright hosts. We set this aperture to the size of an unresolved point source in the HST images ($0.15''$ in diameter). The fixed aperture will include the same amount of light from an unresolved source regardless of its redshift. However, the aperture will contain a larger fraction of the underlying, resolved galaxy for higher redshift objects than for low- z sources. Because of this, the dilution of the nuclear light by the galaxy increases as a function of redshift and, consequently, as a function of nuclear magnitude. If we assume a disk-dominated, $r_e=1$ kpc galaxy containing an AGN that is 10% of the host galaxy light and varying by $\Delta m=0.3$ magnitudes, the measured Δm within our fixed aperture would be 0.15 magnitudes at $z=0.2$ but only 0.06 magnitudes at $z=1$. The observed total nuclear magnitude would drop by ~ 3 magnitudes over this interval. The increasing dilution with redshift is compounded by the increasing photometric errors with magnitude. For an AGN that has varied by $\Delta m=0.3\text{--}0.2$ mags, consistent with typical structure function values for AGN (Trevese *et al.* 1994), and reasonable estimates for the galaxy magnitude, morphology, physical size and true AGN fraction, we estimate that incompleteness due to significant AGN dilution begins to effect our survey at magnitudes between $V_{nuc}\simeq 26.5$ to $V_{nuc}\simeq 27.5$.

As can be seen in Figure 4, all of the variables lie at magnitudes greater than $V_{nuc}=27.3$. While this may partially be due to a real astrophysical effect (see discussion in Section 4), this limiting magnitude is within the range of our incompleteness estimate above. Therefore, although we survey galaxy nuclei to $V_{nuc}\simeq 29$, our limit for detecting *variable AGN* at a uniformly varying level within galaxy nuclei is probably closer to $V_{nuc}\simeq 27.5$, with decreasing completeness fainter than $V_{nuc}\simeq 26.5$.

The 16 variable nuclei detected in our survey represent 2.2% of the galaxies brighter than

$V_{nuc}=29.0$ or 7.4% of the galaxies brighter than $V_{nuc}=27.5$. To emphasize the significance of the variable sources, Figure 5 is a histogram of the sigma distribution for galaxies in the HDF. The X-axis is the absolute value of the normalized magnitude difference (σ) and the Y-axis is the natural logarithm of the number of sources in 0.25σ bins. Errorbars represent the poisson statistical errors. Filled circles show the histogram for all 719 nuclei brighter than $V_{nuc}=29.0$ and open squares represent the 217 nuclei brighter than $V_{nuc}=27.5$. The curved lines are gaussian fits to the data within 2.5σ (solid is the fit to data brighter than $V_{nuc}=29.0$ and dashed is the fit to data brighter than 27.5). In both distributions, the data are well fit by gaussians out to $\sim 3\sigma$ and show a “tail” of significant variables extending to higher σ values. In a normal distribution, we would expect a total of ~ 5 sources to be greater than 3σ brighter than $V_{nuc}=29.0$ with ~ 1.5 expected to lie brighter than $V_{nuc}=27.5$.

Based on Gaussian statistics, we estimate that ~ 1 – 2 of our variables (all detected brighter than $V_{nuc}=27.5$) are spurious, implying that the true number of variables is ~ 14 . If we also correct by 20–25% for incompleteness due to lightcurve sampling, the incompleteness corrected number of variables in the HDF is ~ 18 representing 8.3% of the nuclei brighter than $V_{nuc}=27.5$.

One of the 16 variables detected in this survey, *2-251.0*, was also identified as variable in the I-band variability survey of the HDF (SGP). Eight variables were detected in that survey with significant ($\gtrsim 3\sigma$) magnitude changes over the 2 year time interval (1995–1997). Object *2-251.0* is by far the brightest of these sources, having a nuclear V magnitude $\sim 13\times$ brighter than the next brightest source. Of the 7 I-band variables not detected in the present survey, 5 are fainter than $V_{nuc}=28.0$, placing them below the expected sensitivity limits for this study. The other two I-band variables, *3-266.0* and *3-404.0*, have $V_{nuc}\simeq 27.0$. In the present study, object *3-266.0* changed by 0.025 mag (1.1σ significance) and object *3-404.0* changed by 0.052 mag (2.0σ significance). The latter source is a marginally significant detection and would lie above the 3σ limit if it had been brighter than ~ 26.5 in the V-band. Object *3-266.0*, at just over 1σ significance, may be variable but at lower significance due to the 2-epoch statistical incompleteness effect discussed above.

4. PROPERTIES OF THE SELECTED VARIABLE NUCLEI AND HOST GALAXIES

Figure 6 contains the 1995 V-band images for galaxies with variable nuclei. The postage stamp images are $3''$ on a side and are scaled to the same maximum pixel value. It can be seen from this figure and Table 1 that the selected galaxies cover a range of morphologies, magnitudes and colors. Their redshifts range from 0.09 to 1.8 with a median $\langle z \rangle \simeq 0.66$.

Many of the galaxies have significant bulge components based to the 2-dimensional model fits. We note, however, that several sources with $B/T=0$ also have high chi-square values (>1.25) which in some cases appears to be due to a poorly fit bulge component. In addition to the morphological B/T parameter, we also list the spectral type for the source based upon the photometry of FLY to determine photometric redshifts for galaxies in the HDF. The selected galaxies appear to be evenly distributed over all spectral classes with no particular preference towards early or late-type galaxies.

Figure 7 is a color magnitude diagram of the galaxy nuclei for sources in the HDF. The variable nuclei are indicated with larger solid triangles. The variables cover the full range of $V-I$ colors and do not appear to be preferentially bluer or redder than the non-varying nuclei of galaxies in the HDF.

All of the variables lie at the bright end of the magnitude distribution. As previously discussed, incompleteness due to increasing AGN light dilution as a function of redshift is likely to contribute to this observation. However, an astrophysical effect may be at least partly responsible. AGN are generally found in brighter host galaxies than those that do not harbor AGN (Huchra & Burg 1992; Ho *et al.* 1997; Hamilton *et al.* 2002). If these sources are indeed AGN, we might expect to find them in the brighter galaxies. An additional factor is the inclusion of the AGN light in the nuclear magnitude. We can minimize the above mentioned incompleteness effect by considering only those sources brighter than $V_{nuc}=26.5$, where incompleteness is not expected to be significant. We find that 23% (5/22) of nuclei are variable at $21.8 < V_{nuc} < 25.5$ while only 15% (6/39) are variable at $25.5 < V_{nuc} < 26.5$. While the small numbers do not provide significance, this trend is consistent with the previous studies concerning AGN host galaxies.

5. COMPARISON WITH MULTI-WAVELENGTH HDF SURVEYS

The HDF has been surveyed with a variety of other telescopes and instruments providing a wonderful resource of multi-wavelength information for this particular region of the sky. We have cross-referenced our list of variable nuclei with published catalogs of X-ray, radio and far-infrared sources as well as other photometric and spectroscopic surveys used to search for nuclear activity.

AGN have long been recognized as X-ray sources, being associated with a wide range of activity levels from the brightest quasars to low-luminosity Seyferts. Even highly obscured AGN can often be detected at X-ray wavelengths. Some of the light obscured by dust at other wavelengths will be reprocessed and emitted in the mid-IR. For these reasons, the

X-ray and mid-IR regimes are excellent wavelengths in which to detect and study AGN.

Recent deep surveys with the Chandra X-ray Observatory have resolved many X-ray sources in the HDF and provide information about the nature of the X-ray radiation. The 2Ms Chandra X-ray survey (Alexander *et al.* 2003) has detected 20 sources in the original HDF and an additional 2 sources of lower significance which are listed in their supplementary catalog. Of these 22 detections, 18 are included in our variability study. Two were not included because their optical fluxes were too faint to be included in our survey and an additional pair fell too close to the edge of the CCD to obtain accurate nuclear photometry in both epochs. Of these 18 sources, we find seven that match (within $1.2''$) the positions of our variable nuclei (see columns 10 and 11 of Table 1). The filled symbols in Figure 4 represent the 18 X-ray sources included in our survey and show the level of variability significance for each source.

In addition, we have found several variables coincident with source positions from the ISOCAM $15\mu\text{m}$ survey of the HDF (Aussel *et al.* 1999) and the 1.4GHz radio survey (Richards *et al.* 1999). These are listed in columns 12 through 14 of Table 1. Below, we discuss the variable galaxy nuclei that overlap with one or more of these multi-wavelength surveys.

2-251.0: This $z=0.960$ early-type spiral galaxy is one of only two broad-line AGN in the HDF (see Section 6) and is a bright X-ray source detected with Chandra in the soft, hard and ultrahard bands (Hornscheiwer *et al.* 2000; Brandt *et al.* 2001a – hereafter H00, B01a) with a photon index of 0.67. We detect it as an optical variable at 6.5σ significance. As previously mentioned, it is the only object that was also detected in our I-band survey of the HDF (SGP). Spectroscopic detection of broad MgII (Phillips *et al.* 1997), as well as 1.4GHz radio (Richards *et al.* 1999a) and ISOCAM (Aussel *et al.* 1999) detections for this source all corroborate the AGN nature of this galaxy. Spectral fitting of the X-ray data has revealed a large intrinsic column density which appears to be related to the AGN (B01a).

3-355.0: This elliptical galaxy at $z=0.474$ is a 3.2σ variable. The original 166ks Chandra exposure did not detect this source in the hard band, but B01a report hard X-ray counts from the deeper 479.7ks exposure. The photon index determined from the 2Ms exposure is 1.8. This galaxy is also a radio source with a steep radio spectrum ($\alpha=1.0$). Its position is coincident with an ISO source from the Aussel *et al.* (1999) supplementary table of lower significance detections. H00 note that the X-ray luminosity for this source is consistent with that expected from hot gas in an elliptical but the nuclear variability detected here suggests this galaxy may also host an AGN.

3-659.1: The variable source is a spiral galaxy at $z=0.401$ (Barger *et al.* 2002) with a

variability significance of 4σ . This optical galaxy is $\sim 1.2''$ from the hardest X-ray source ($\Gamma=0.56$) in the HDF. The X-ray position is only $0.22''$ from the second reddest source in the HDF NICMOS survey (Dickinson *et al.* 2000). Even though the optical galaxy is positioned further from the center of the X-ray emission, the detected variability suggests that perhaps some of the X-ray emission originates from the galaxy nucleus. There is also significant 1.4GHz radio emission (Richards *et al.* 1999a) and $15\mu\text{m}$ emission detected with ISO (Aussel *et al.* 1999). The radio position is again more closely aligned with the NICMOS source than the optical galaxy (see Figure 1 in Richards 1999b) but both the NICMOS and optical sources are within the positional uncertainties.

3-965.111111: This is the most significant variable in our survey (9.4σ). It was not detected in either the radio or mid-IR bands and was first detected in the 1Ms Chandra survey (Brandt *et al.* 2001b). It was detected in both the soft and hard X-ray bands in the 2Ms survey and has a photon index of 0.91. It is a bright elliptical galaxy near the edge of the HDF at $z=0.663$.

4-752.1: This optically variable (3.1σ) X-ray source is also an FR I radio galaxy (Richards 2000) with extensive radio structure. The host galaxy is a red elliptical at $z=1.05$. This source has not been detected in the hard X-ray band and thus appears to fall into the low X-ray luminosity/soft X-ray spectrum grouping of very red objects (Hogg *et al.* 2000). Because of its faintness, the photon index cannot be determined. B01a suggests that the X-ray emission is associated with the central AGN or the hot interstellar medium and X-ray binaries of the elliptical galaxy. It is not detected in the mid-infrared.

4-976.1: This bright spiral galaxy at $z=0.089$ is variable at the 3.6σ significance level. B01a notes that the position of the X-ray source is not coincident with the galaxy nucleus (which is $1.1''$ away) but does lie near ($\sim 0.14''$) an off-nuclear bright spot. They suggest that this bright spot may be a background AGN, starbursting region, or “super Eddington” X-ray binary (B01a, H00). Our variability measurements have been made on the central nuclear region of this galaxy which, if hosting an AGN, may be responsible for at least part of the X-ray emission. The photon index for this source is 1.7. This galaxy is within $3.3''$ of a mid-IR source (Aussel *et al.* 1999).

3-386.111: This is a spiral galaxy at $z=0.474$ which is listed in the 2Ms X-ray survey supplementary catalog containing lower significance sources associated with optically bright objects. The nucleus has a variability significance of 3.8σ . This source was not detected in the hard X-ray band. It is associated with an ISO source listed in the supplementary ISO source catalog.

One additional variable nucleus, *4-254.0*, matched the position of a lower significance

X-ray source indicated in the 1.38Ms Chandra survey (Brandt *et al.* 2002). This X-ray source, however, was not listed among the 2Ms detections. The object is an elliptical galaxy at $z=0.901$ which is also associated with an ISO detection in the supplementary catalog.

Of the remaining 8 variable nuclei, one (*2-860.0*) is associated with a mid-IR detection and another (*3-943.0*) is within $\sim 2''$ of a 1.4GHz radio source. The other 6 are not associated with any of the multi-wavelength surveys discussed here.

Overall, 44% (7/16) of our variable galaxy nuclei have X-ray counterparts from the 2Ms Chandra survey (or 31% excluding the two matches with greatest positional offsets). Optical variables make up 39% of the X-ray sources. Of the brightest X-ray sources (full-band flux $\geq 2.4 \times 10^{-16}$ ergs/s) five out of nine (56%) are associated with optical variables. If we assume that the observed optical variability indicates the presence of an AGN, this is an important check on the nature of the X-ray emitting source and could potentially help discriminate between low-luminosity X-ray emitting AGN and other X-ray emitting phenomena such as supernova remnants or X-ray binaries. There does not appear to be a relation between photon index and the detection of optical variability. Five of the eight X-ray sources in the HDF with enough signal to determine photon indices are optical variables. The X-ray/optical variables make up two of the softer X-ray sources and three of the harder sources in this small sample.

Seven of our 16 variables are associated with mid-IR detections (44%) and five (31%) have radio emission at 1.4GHz. Variable galaxies make up 22% of the detected sources at $15\mu\text{m}$. This is comparable to the portion of the mid-IR integrated light attributed to AGN based on the correlation of mid-IR sources with Chandra sources (Elbaz *et al.* 1999).

Finally, we have compared our results with two photometric studies to identify QSOs in the HDF on the basis of multi-band colors. Jarvis & MacAlpine (1998) identified 12 high redshift ($z>3.5$) QSO candidates. Eleven of these sources were included in our variability survey but none showed significant variability amplitudes, having a median σ of ~ 0.6 . Based on structure functions for AGN/QSOs (Trevese *et al.* 1994; Hook *et al.* 1994; Hawkins *et al.* 2002) and taking into account time-dilation effects ($\Delta t_{rest} = \Delta t / (1+z)$), the average magnitude change expected in our survey for high- z QSOs is ~ 0.1 – 0.2 magnitudes. Even sources dominated by an AGN component, as expected for these color-selected candidates, would be difficult to detect above the 3σ significance threshold due to their faint apparent magnitudes ($V_{nuc} \gtrsim 27.7$). Nonetheless, an average magnitude change of only ~ 0.05 is significantly less than the 0.1 – 0.2 average magnitude change predicted from QSO structure functions.

Conti *et al.* (1999) also identify 20 compact sources having QSO-like colors and mor-

phologies with estimated redshifts between $z \sim 1$ and 5.5. The nuclear magnitudes for these objects lie at $V_{nuc} \simeq 27\text{--}28$. None were identified as variable above the 3σ threshold in our survey. The average nuclear magnitude of this sample is ~ 1 magnitude brighter than the Jarvis & MacAlpine QSOs. If these are variable QSOs/AGN-dominated galaxies, we would again expect an average magnitude change of $\sim 0.1\text{--}0.2$. The average change in magnitude for the Conti *et al.* sample over the 5 year interval is ~ 0.03 magnitudes, with all sources lying well below the 2σ significance limit.

6. OPTICAL SPECTRA

The extensive redshift surveys of the HDF from Cohen *et al.* (1996; 2000), Phillips *et al.* (1997) and Barger *et al.* (2002) have revealed only two broad-line AGNs (BLAGNs) in the HDF proper. These are *2-251.0* ($z=0.96$ variable galaxy and X-ray source discussed above) and *4-852.12* ($z=0.943$ X-ray source). The measured variability significance of *4-852.12* is 0.35σ . It is possible that this source is variable but has been observed at two points in its light curve that are close to the same magnitude. Further monitoring of the HDF would be necessary to rule out optical variability for this BLAGN.

We have studied the available spectra for all of the galaxies hosting variable nuclei to determine if any of the sources show specific emission lines or line flux ratios indicative of Type 2 AGN. Of the 16 variables, optical spectra exist for 13. One of these is the BLAGN *2-251.0* already discussed, which shows broad MgII ($\lambda 2800$) emission and absorption in its spectrum. Almost all of the remaining 12 show emission lines in their spectra. Nine out of 11 show OII($\lambda 3727$) when in range, with several sources also displaying H β and OIII($\lambda 5007$). The X-ray and strong radio FR II galaxy *4-752.1*, displays only strong absorption lines in its spectrum. Only one source, *4-254.0*, shows weak NeV($\lambda 3426$) emission, a line indicative of the presence of an AGN (Hall *et al.* 2000). NeIII($\lambda 3869$), also stronger in AGN than in starforming galaxies (Rola *et al.* 1997), is seen weakly in 2 sources, *3-143.0* and *3-386.111111*. These galaxies also show OIII and H β , but with flux ratios consistent with star formation rather than AGN activity (Veilleux & Osterbrock 1997). Only the spiral galaxy *4-976.1* is low enough redshift to reveal strong H α , SII($\lambda 6713+6731$) and OI($\lambda 6300$) emission in the optical spectrum. The line flux ratios of OIII/H β , SII/H α and OI/H α all indicate that this source is near the border that divides starforming galaxies and AGN (Veilleux & Osterbrock 1997). Therefore, based on the optical spectra alone, objects *2-251.0* (BLAGN), possibly *4-976.1* (LINER/Seyfert 2), and possibly *4-254.0* (through the weak presence of NeV) show evidence of AGN.

7. LUMINOSITY FUNCTION FOR VARIABLE NUCLEI

Knowledge of the space density of faint AGN at higher redshifts is critical to our understanding of AGN evolution and the AGN phenomenon in general. Our sample of 16 variable sources spans a redshift range of $z=0.1$ to 1.8 with most sources lying between $z=0.4$ and 1.1 . If we make the assumption that these variables are indeed AGN, it is interesting to compare their number density with local samples of AGN.

We must first estimate the luminosity of the AGN candidates in our survey. Due to the faint magnitudes and small angular sizes of many of the variables, 2-dimensional modeling to separate the components (disk+bulge+AGN) of the galaxies is difficult and would not yield consistent results for all of the selected galaxies. A simpler approach is to estimate the AGN luminosities by assuming that the entire nuclear flux is attributed to the AGN. This value is an overestimate in one sense since the nuclear light will also include light from the underlying galaxy, though the small nuclear aperture minimizes the contribution from the host. Based on the expected level of variability over this time interval predicted from AGN structure functions, we estimate the variable component for our AGN candidates to be no less than 15% of the total nuclear light. In the most extreme case, the true AGN magnitude could be ~ 2 magnitudes fainter than that measured within the nuclear aperture. In another sense however, we underestimate the AGN flux since we have not applied aperture corrections to include light from the wings of the PSF. Our aperture of $r=0.075''$ encircles about 50% of the flux from a point source (Holtzman *et al.* 1995). If the point source makes up the entire flux within the aperture, an aperture correction would increase the magnitude by up to ~ 0.8 mag. If the point source is some fraction of the total nuclear light, the aperture correction will be smaller. Determining the true aperture correction is not possible without knowing the relative fluxes of the point source and host within the fixed aperture.

Figure 8 is the absolute magnitude based on the nuclear flux *vs* the source redshift ($H_o=75$ km/s/Mpc; $q_o=0.5$). The absolute B magnitudes are calculated assuming a power-law index of $\alpha=-1.0$ resulting in a K-correction of zero and $V_{F606W}-B_J=-0.32$. We find that most sources lie between $-15 \gtrsim M_B \gtrsim -17$ in the redshift range $0.4 < z < 1.1$.

We conduct the Luminosity-Volume test, or V/V_{max} test, of Schmidt (1968) to determine if significant evolution is present in our sample of variable nuclei. For this calculation, we determine for each source in our survey the maximum redshift at which it could exist and still be included in our survey. The volume of space enclosed by a sphere with a radius equal to this z_{max} is the value V_{max} . The volume enclosed at the true redshift of the source is V . Spectroscopic redshifts have been determined for 14 of our objects. Photometric redshifts are estimated for one other (FLY). There is no spectroscopic or photometric redshift published for 2-456.22. Based on the V-I color for this object, we estimate its photometric redshift to

be $z=1.8$ which corresponds to those of other HDF sources with similar colors.

To define z_{max} , we determine the limiting redshift for each source to be detected in our survey. The brightest limiting magnitude in our survey is defined by the 3σ line in Figure 4a, which indicates the faintest magnitude at which a source varying by a given Δm would be considered a significant variable. Below this magnitude, a source varying by Δm would not be detected as variable. Therefore, z_{max} is the redshift where the apparent magnitude of a nucleus varying by Δm falls below the 3σ variability significance limit shown in Figure 4a.

The mean V/V_{max} for the 16 nuclei in our survey is 0.67 ± 0.07 . For a population of objects uniformly distributed in space, $\langle V/V_{max} \rangle = 0.5$. Our value of 0.67 ± 0.07 indicates that sources are found more often at larger distances than at nearby distances, indicating some evolution in the population of galaxies with variable nuclei. Our survey incompleteness, as discussed in Section 3, affects our ability to detect sources at higher redshifts and fainter magnitudes. Thus, the value of $\langle V/V_{max} \rangle$ would actually be higher if corrected for this incompleteness. An increase in the number density would be consistent with the picture of AGN/QSO evolution at higher luminosities, where the population increases rapidly out to $z \simeq 3$.

Even though evolution may be present among our sample, the small number of sources spread over a range in redshift makes it difficult to construct the luminosity function in more than one redshift bin. To accurately compare the density of our sources to local samples, we construct the LF in one redshift bin at $z=0.4-1.1$. We choose these limits to minimize the redshift range of our sources while maximizing the number of sources in the bin. Twelve of our 16 sources lie within this redshift range, which excludes the 2 lowest and highest redshift galaxies. The mean redshift for these sources is $\langle z \rangle = 0.69$.

We calculate the luminosity function using a technique similar in nature to the V/V_{max} test described above. The LF is created by summing $1/V_{max}$ for sources in discrete magnitude bins. In this case, we are actually determining V_a , or the *accessible* volume in which each source could be detected. This volume is limited not only by the magnitude limit for detection, but also by the lower and upper redshift limits of the shell in which we are summing. Figure 9 is the LF for HDF variable nuclei in the redshift range $z=0.4-1.1$. Incompleteness due to the fact that our variability selection is based on only 2 epochs is expected to produce an underestimate in the number of AGN by a factor of ~ 1.3 , or a decrease in $\log \phi$ of ~ 0.12 . For comparison, we plot the local Seyfert LFs of Huchra & Burg (1992; HB92) from the CfA survey and Ulvestad & Ho (2001; UH01) from the Palomar survey. Both local surveys consist of spectroscopically selected Seyfert 1s and 2s.

Our LF for variable sources at $0.4 < z < 1.1$ extends to fainter absolute magnitudes than the local LFs, largely due to the fact that the local LFs are calculated for the total galaxy light (AGN+host) rather than the magnitude of the AGN alone. Nonetheless, many of the AGN candidates detected in our survey may be truly fainter than those of HB92. Based on the spectroscopic selection criterion employed by HB92, most of our sources would not be detected as AGN (see Section 6) in the HB92 survey. Therefore, we assume that the AGN component in our galaxies do not comprise as much of the total galaxy light as the HB92 sources and are likely to be intrinsically fainter.

The UH01 LF covers the same integrated galaxy magnitude range as HB92 but shows an overall higher density for local Seyferts. Ulvestad & Ho explain that this is due to the fact that their LF includes intrinsically fainter seyfert nuclei than does the HB92 sample. For the Seyfert 1 galaxies, Ho & Peng (2001) decompose the nuclei from the host galaxies in both local samples and confirm this assertion, finding a median nuclear magnitude of $M_B = -14.6$ for UH01 versus -17.4 for the HB92 Seyfert 1 galaxies. From their study, we also find that the nuclear magnitudes of the local seyferts in both samples can be extremely faint when compared to the total galaxy magnitude, in some cases up to 10 magnitudes fainter. Therefore, an LF consisting of nuclear magnitudes for local Seyferts would be a much better comparison to our HDF AGN candidates.

Since this is not currently available, an alternative is to produce the LF of our sources using the total integrated galaxy magnitude rather than the nuclear magnitude alone (dashed LF). The integrated galaxy magnitudes for our variable sources cover the same range as the faint end of the local Seyfert LFs but have a number density $6\text{--}10\times$ greater than the local Seyfert density of UH01. If the AGN in these two samples cover a similar magnitude range, this is evidence for a significant increase in number density from $z=0$ to ~ 0.7 . The magnitudes for the UH01 AGN determined in Ho & Peng (2001) for the Seyfert 1 population cover the range $-9 \gtrsim M_B \gtrsim -22$ mag with most lying within $-12 \gtrsim M_B \gtrsim -20$. Our nuclear aperture LF (open circles in Figure 9) extends from $-14.5 \gtrsim M_B \gtrsim -19$. In the most extreme case, based on the over and underestimates of the true AGN magnitudes discussed previously, the variable AGN in our survey could cover the magnitude range $-12.5 \gtrsim M_B \gtrsim -20$. This magnitude range is consistent with that estimated for the UH01 sample. It is therefore unlikely that the increase in number density between the UH01 LF and our LF is due to the inclusion of intrinsically fainter AGN as appears to be the case for the difference between the UH01 and HB92 LFs.

Finally, we note that the LF for the variable nuclei continues to rise at faint magnitudes, indicating that number counts have not begun to turn over at magnitudes even as faint as $M_B \sim -15$. The effects of incompleteness in our survey due to AGN light dilution would cause

us to be less complete at the faint end and corrections in this sense would likely increase rather than decrease our faintest LF bin. Most local AGN LFs, such as those shown in Figure 9, show a flattening toward fainter magnitudes. The local LF of Londish *et al.* (2002) for type 1 AGN reveals a much flatter slope at the faint end as compared to the bright end and can be well fit with a two power-law function. Our increasing numbers at the faint end may be an evolutionary effect or might be attributed to the inclusion of a greater fraction of obscured AGN. More data are needed as well as better classification into AGN types to improve the statistics and verify this trend.

8. SUMMARY AND CONCLUSIONS

We have investigated variability within the Hubble Deep Field North with the aim of identifying low-luminosity AGN in the nuclei of field galaxies. We compare photometry of the nuclei of galaxies in the initial V-band image obtained in 1995 and a second image obtained in 2000 and find evidence for significant variability in 16 galaxies. Correcting for possible spurious detections and incompleteness results in a total of ~ 18 sources which make up 8.3% of galaxy nuclei to $V_{nuc}=27.5$. The galaxies hosting variable nuclei range in redshift from $0.09 < z < 1.8$ with most lying between $0.4 < z < 1.1$. Nuclear colors of the variable nuclei are consistent with those of non-variable nuclei.

Seven of our variable sources are coincident (within $\sim 1.2''$) with X-ray sources detected in the 2Ms Chandra exposure (Alexander *et al.* 2003). We find that 39% of the 2Ms Chandra detections in the original HDF are significant variables. The optical variability observed in these X-ray sources provides important evidence to confirm the presence of an AGN and could potentially help discriminate between low-luminosity X-ray emitting AGN and other X-ray emitting phenomena such as supernova remnants or X-ray binaries. In addition, 44% of our sources are associated with mid-IR detections at $15\mu\text{m}$ and 31% are detected at 1.4GHz.

Optical spectra are currently available for 13 of the 16 variable sources. Object *2-251.0* is a broad-line AGN. Two others show some evidence of harboring an AGN. Object *4-976.1*, a low redshift spiral, has emission line ratios indicative of a LINER/Seyfert 2 and *4-254.0* reveals weak NeV emission.

Based on the V/V_{max} test, there is evidence for evolution within our sample of variable nuclei in the sense that more variables are found at higher redshifts. We estimate the luminosity function of variable AGN in the redshift range $0.4 < z < 1.1$. This LF is a lower-limit since our variability selection technique, employing only 2 epochs for detection, could

miss $\sim 20\text{--}25\%$ of variable nuclei. The nuclear magnitudes for our variables extend to $M_B \simeq -15.0$ with a median magnitude of $M_B = -16.3$. Computing our LF with total integrated galaxy magnitudes, we compare to the LF of Ulvestad & Ho (2001) for local Seyfert galaxies. If our AGN cover a similar magnitude range as those included in their sample, we find evidence for an increase in the number density of faint AGN by a factor of 6–10 from $z \sim 0$ to 0.7. The LF for our selected variable nuclei continues to rise at faint magnitudes. Unlike the LFs of most QSOs and local Seyferts, we do not see signs of flattening at the faint end.

The results of this paper can be tested and confirmed with a larger sample of variable nuclei detected at these redshifts. A similar variability survey is being conducted for the Groth-Westphal Survey Strip (Sarajedini *et al.* 2003) over 7 years and will produce a larger sample of variables to improve the statistical significance of any evolutionary trends. Additional future work includes the analysis of the currently ongoing GOODS HST Treasury program (Dickinson *et al.* 2003), an ACS survey of the sky around and including the HDF. The 5-epoch survey, at intervals of ~ 45 days, will allow for the investigation of short-term variability as well as providing confirmation and improved completeness for the variables detected in this study.

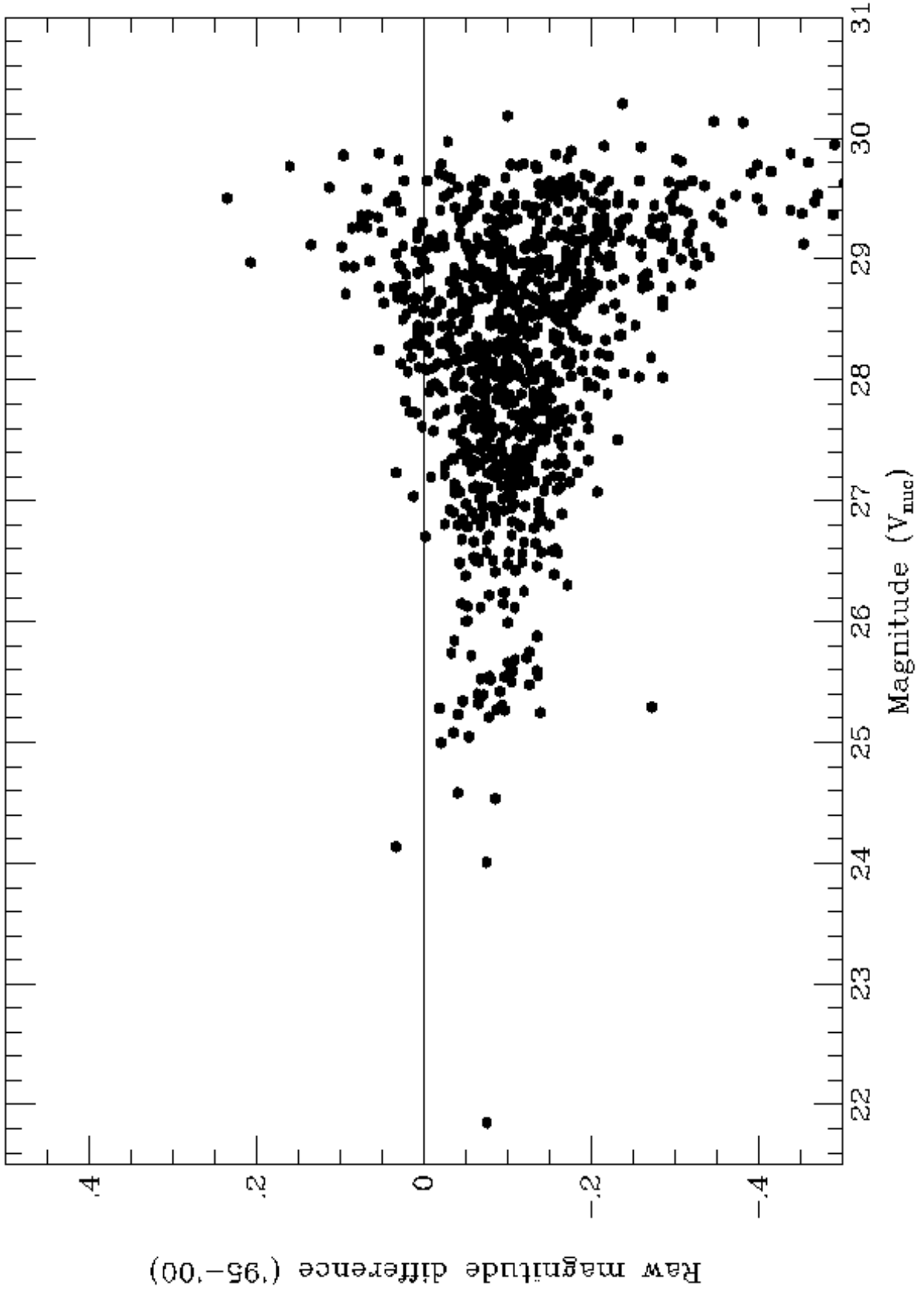
Support for proposal GO-8389.02-97A for VS and GO-8389.01-97A and AR-7984.01-96A for RG was provided by NASA through a grant from the Space Telescope Science Institute, which is operated by the Association of Universities for Research in Astronomy, Inc., under NASA contract NAS5-26555. We gratefully thank Rodrigo Ibata who was the PI for obtaining the second epoch V-band image of the HDF. A special thanks to Amy Barger and Judy Cohen for supplying the Keck spectra in digital form to be analyzed for these sources. Thanks also to David Koo and the referee for helpful comments and suggestions for improving this paper.

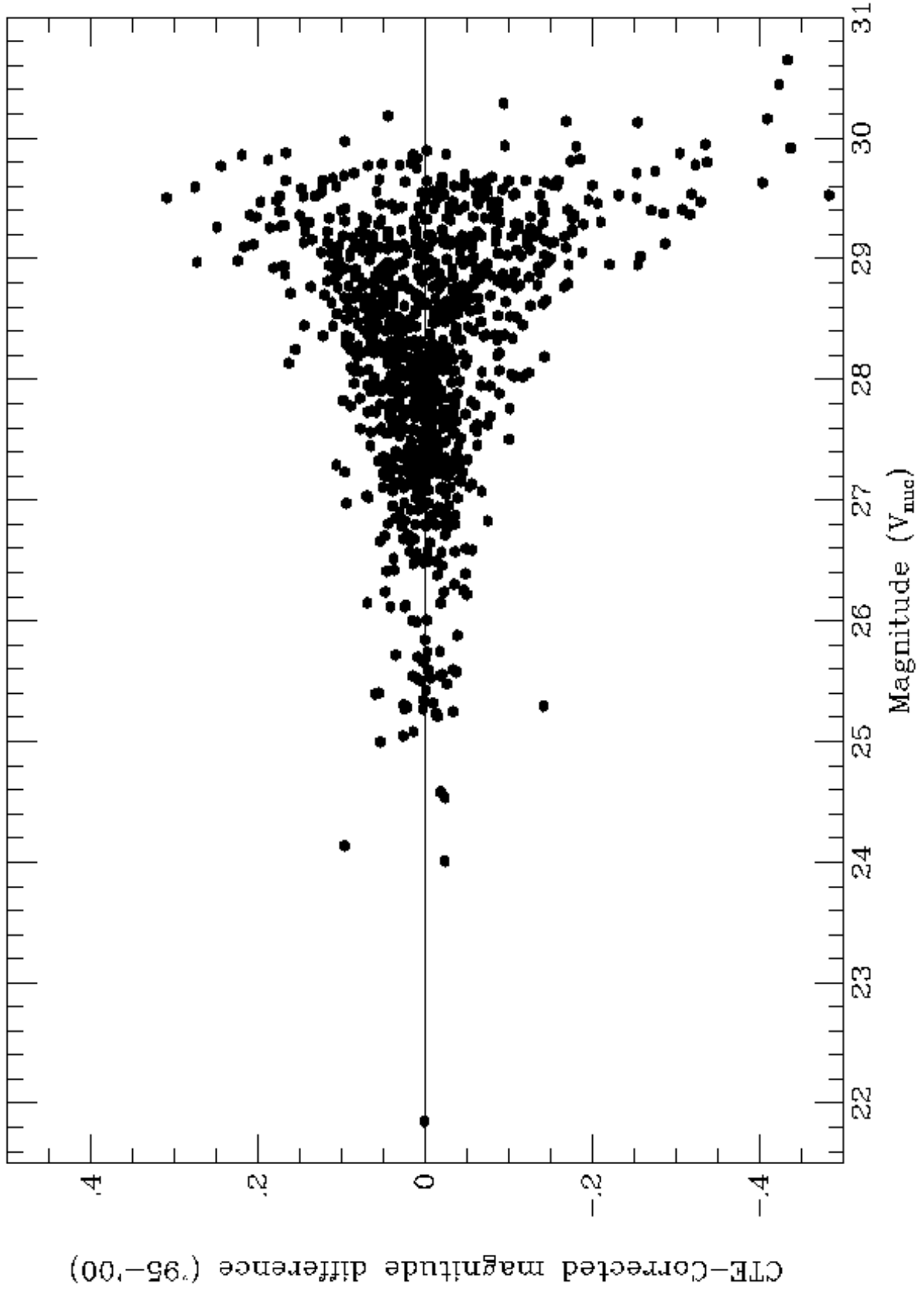
REFERENCES

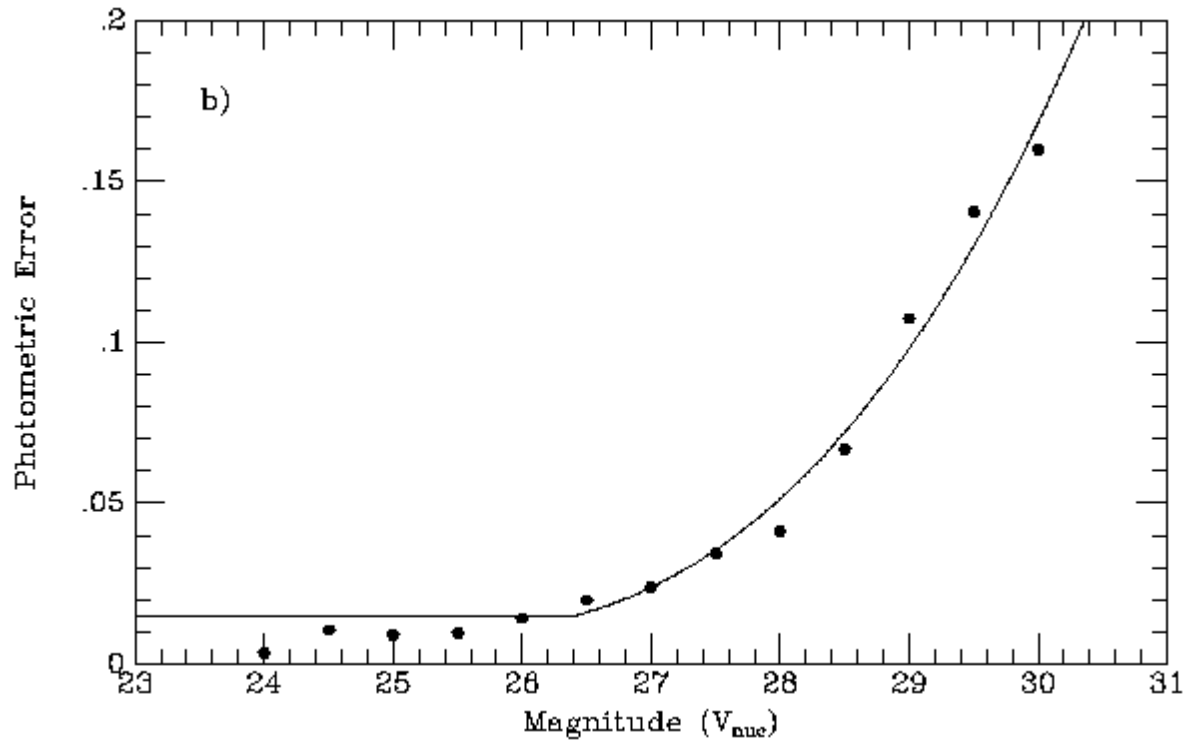
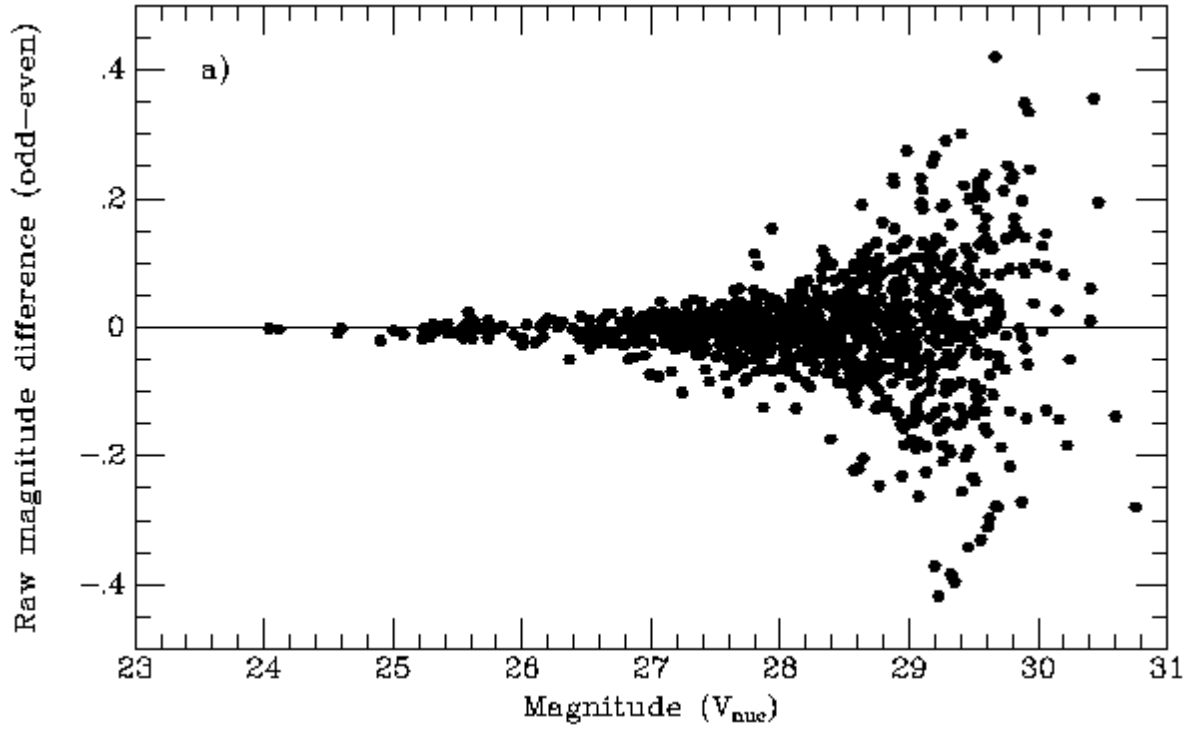
- Alexander, D. M. *et al.* 2003, ApJ, in press (astro-ph/0304392)
- Aussel, H., Cesarsky, C. J., Elbaz, D., & Starck, J. L. 1999, A&A, 342, 313
- Barger, A. J., Cowie, L. L., Brandt, W. N., Capak, P., Garmire, G. P., Hornschemeier, A. E., Steffen, A. T., & Wehner, E. H. 2002, AJ, 124, 1839
- Barger, A. J., Cowie, L. L., Capak, P., Alexander, D. M., Bauer, F. E., Brandt, W. N., Garmire, G. P., & Hornschemeier, A. E. 2003, ApJL, 584, 61
- Bershady, M. A., Trevese, D., & Kron, R. G. 1998, ApJ, 496, 103
- Biretta, J., Baggett, S., Riess, A., Schultz, A., Casertano, S., Gonzaga, S., Heyer, I., Koekemoer, A., Mack, J., McMaster, M. 2001, BAAS, 198, 402
- Boyle, B. J., Shanks, T., Croom, S. M., Smith, R. J., Miller, L., Loaring, N., Heymans, C. 2000, MNRAS, 317, 1014
- Brandt, W. N. *et al.* 2001a, AJ, 122, 1 (B01a)
- Brandt, W. N. *et al.* 2001b, AJ, 122, 2810
- Brandt, W. N., Alexander, D. M., Bauer, F. E., Hornschemeier, A. E. 2002, in Philosophical Transactions of the Royal Society (Series A: Mathematical, Physical, and Engineering Sciences), 360, 2057
- Bunker, A., Spinrad, H., Stern, D., Thompson, R., Leonidas, M., Davis, M., & Dey, A. 2000 (astro-ph/0004348)
- Cheng, F. Z., Danese, L., De Zotti, G., & Franchesini, A. 1985, MNRAS, 212, 857
- Cohen, J. G., Hogg, D. W., Blandford, R., Cowie, L. L., Hu, E., Songaila, A., Shopbell, P., and Richberg, K. 2000, ApJ, 538, 29
- Cohen, J. G., Cowie, L. L., Hogg, D. W., Songaila, A., Blandford, R., Hu, E., & Shopbell, P. 1996, ApJL, 471, 5
- Conti, A., Kennefick, J. D., Martini, P., & Osmer, P. S. 1999, AJ, 117, 645
- Dickinson, M., *et al.* 2000, ApJ, 531, 624
- Dickinson, M., *et al.* 2003, in "The Mass of Galaxies at Low and High Redshift", proceedings of the ESO Workshop held in Venice, Italy, 24-26 October 2001, 324
- Elbaz, D., *et al.* 1999, A&A, 351, 37
- Fernández-Soto, A., Lanzetta, K.M., & Yahil, A. 1999, ApJ, 513, 34 (FLY)
- Giveon, U., Maoz, D., Kaspi, S., Netzer, H., & Smith, P. S. 1999, MNRAS, 306, 637

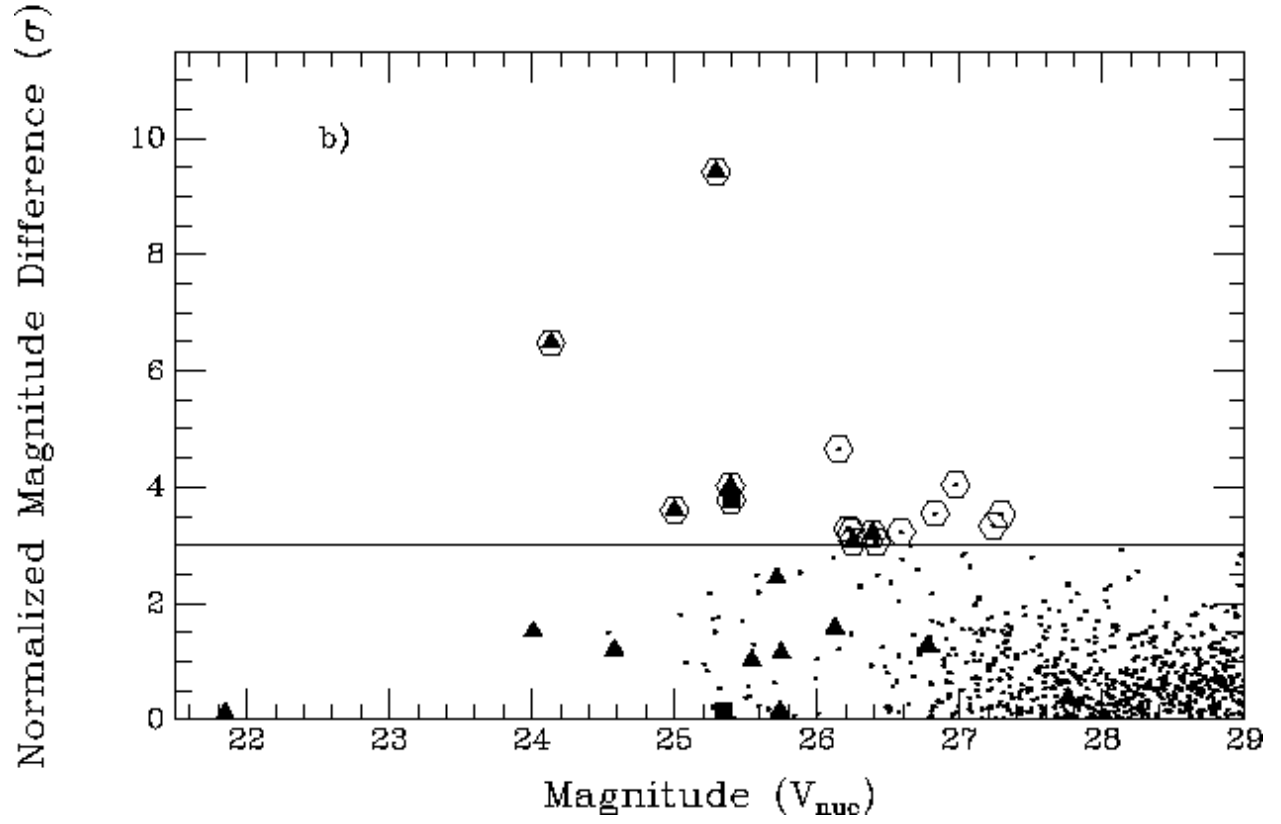
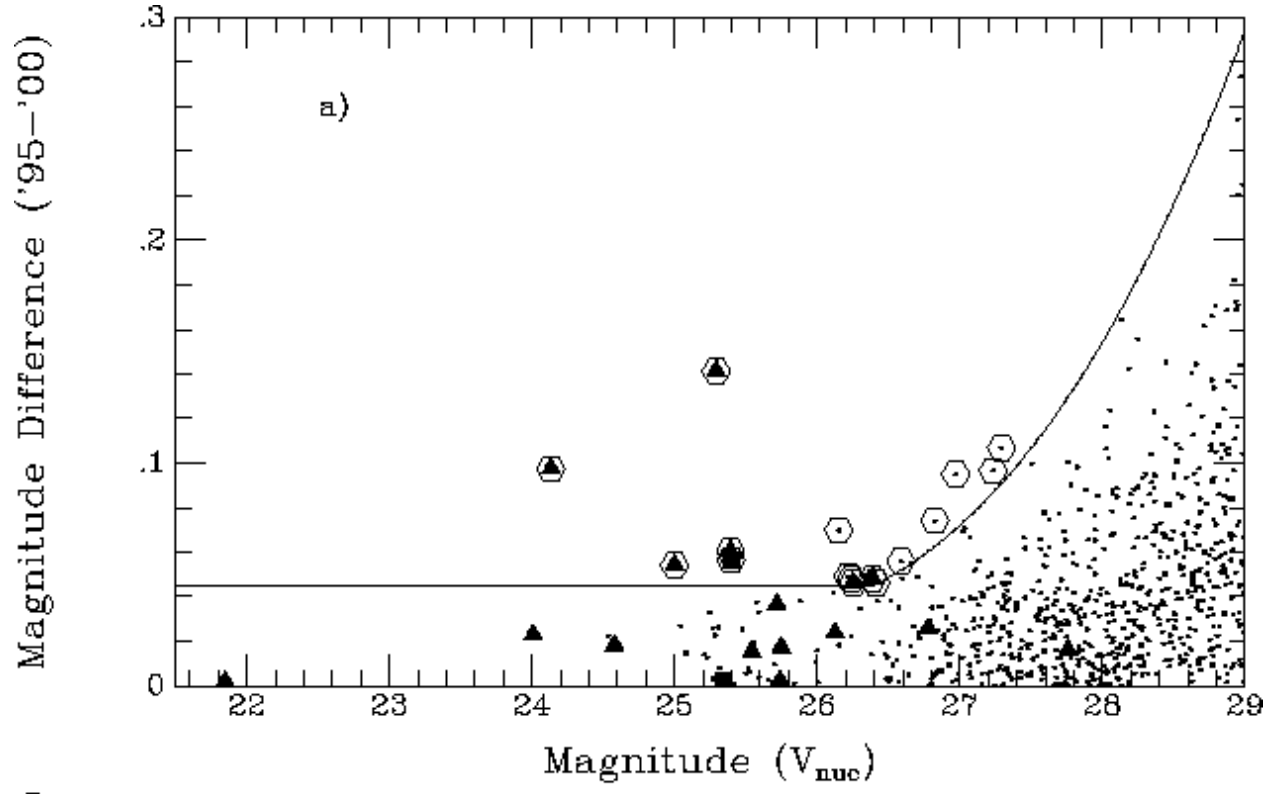
- Gilliland, R. L., Nugent, P. E., & Phillips, M. M. 1999, ApJ, 521, 30
- Hall, P. B. *et al.* 2000, AJ, 120, 2220
- Hartwick, F. D. A. & Schade, D. 1990, ARA&A, 28, 437
- Hawkins, M. R. S. 1986, MNRAS, 219, 417
- Hawkins, M. R. S. 2002, MNRAS, 329, 76
- Holtzman, J. A. *et al.* 1995, PASP, 107, 156
- Huchra, J. & Burg, R. 1992, ApJ, 393, 90 (HB92)
- Ho, L.C., Filippenko, A., & Sargent, W.L.W. 1997, ApJS, 112, 315
- Ho, L. C. & Peng, C. Y. 2001, ApJ, 555, 662
- Hogg, D. W., *et al.* 2000, ApJS, 127, 1
- Hook, I. M., McMahon, R. G., Boyle, B. J., Irwin, M. J. 1994, MNRAS, 268, 305
- Hornschemeier, A. E. *et al.* 2000, ApJ, 541, 49 (H00)
- Jarvis, R. M. & MacAlpine, G. M. 1998, AJ, 116, 2624
- Koehler, T., Groote, D., Reimers, D., & Wisotzki L. 1997, A&A, 325, 502
- Koo, D. C., Kron, R. G., & Cudworth, K. M. 1986, PASP, 98, 285
- Londish, D., Boyle B. J., & Schade, D. J. 2000, MNRAS, 318, 411
- Maiolino, R. & Rieke, G. H. 1995, ApJ, 454, 95
- Marleau, F. R. & Simard, L. 1998, ApJ, 507, 585
- Phillips, A.C. *et al.* 1997, ApJ, 489, 543
- Richards, E. A., Fomalont, E. B., Kellermann, K. I., Windhorst, R. A., Partridge, R. B.,
Cowie, L. L. and Barger, A. J. 1999a, ApJL, 526, 73
- Richards, E. A. 1999b, ApJL, 513, 9
- Richards, E. A. 2000, PASP, 112, 1001
- Rola, C. S., Terlevich, E., & Terlevich, R. J. 1997, MNRAS, 289, 419
- Sarajedini, V. L., Gilliland, R. L., & Phillips, M. M. 2000, AJ, 120, 2825 (SGP)
- Steidel, C. C. & Sargent, W. L. W. 1989, ApJL, 343, 33
- Schirber, M. & Bullock, J. S. 2003, ApJ, 584, 110
- Trevese, D., Kron, R. G., Majewski, S. R., Bershadsky, M. A., & Koo, D.C. 1994, ApJ, 433,
494
- Ulvestad, J. S. & Ho, L. C. 2001, ApJ, 558, 561 (UH01)

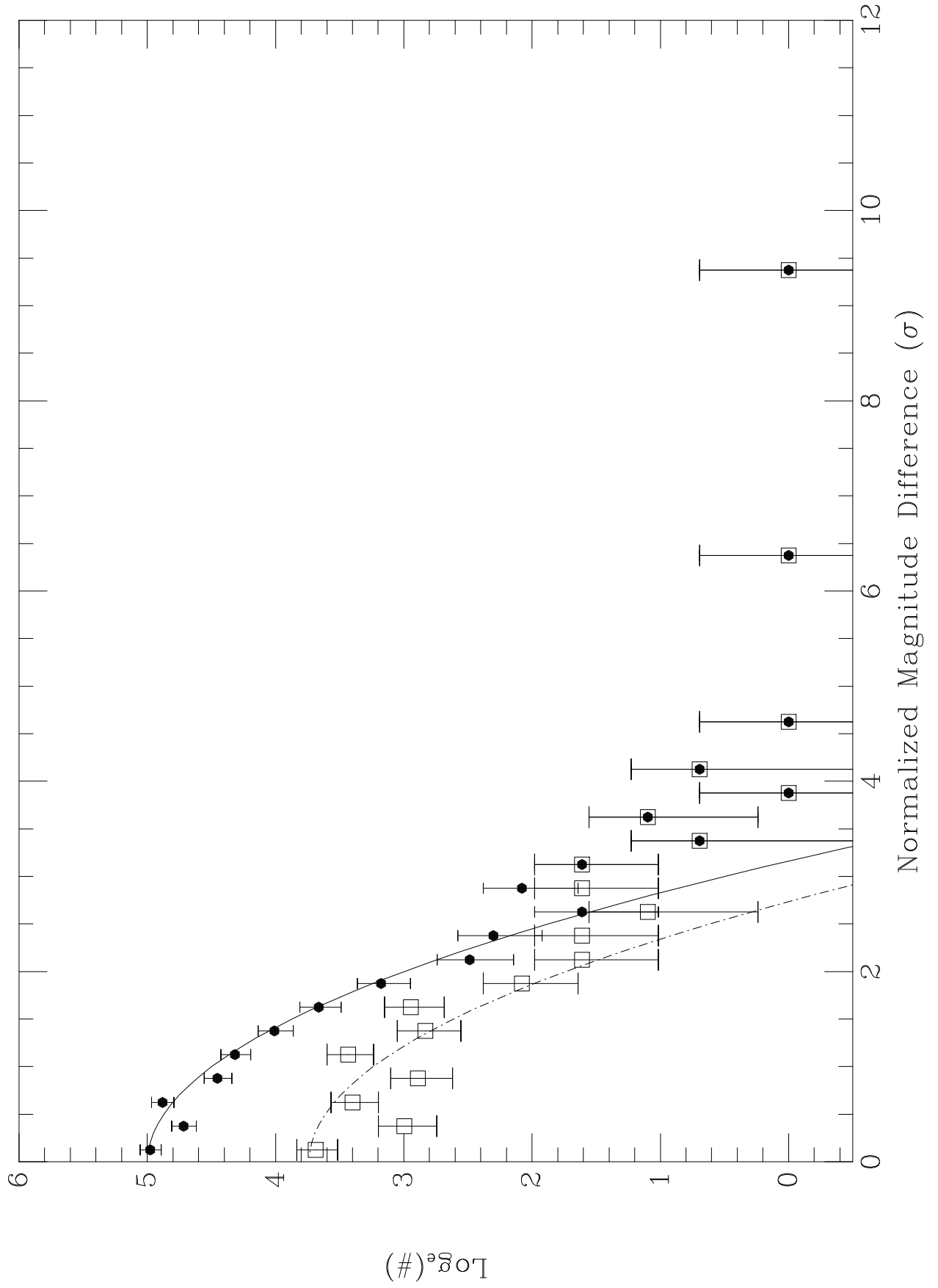
- Veilleux, S. & Osterbrock, D. E. 1987, ApJS, 63, 295
- Whitmore, B., Heyer, I., Casertano, S. 1999, PASP, 111, 1559
- Williams, R.E. *et al.* 1996, AJ, 112, 1335

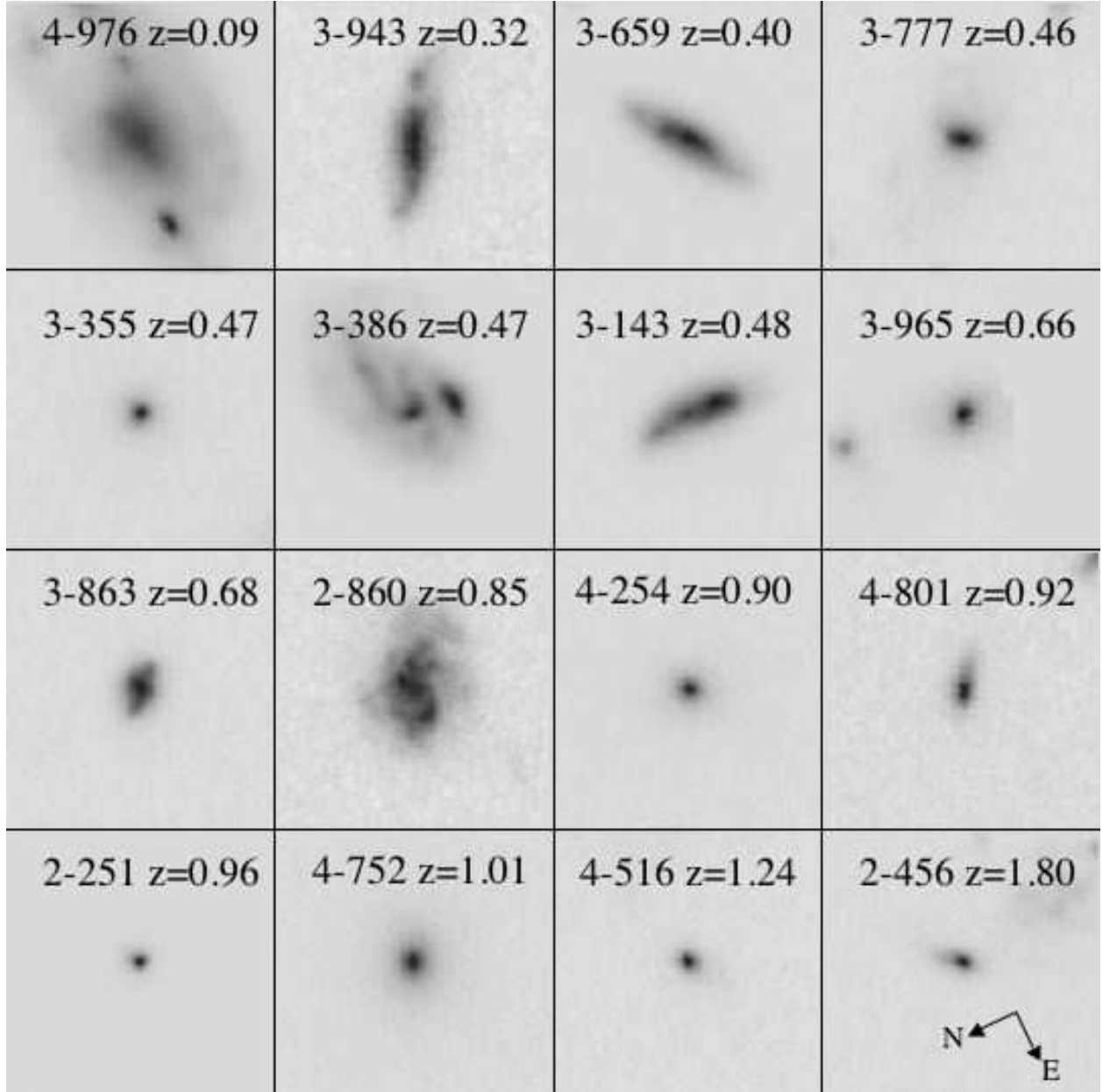


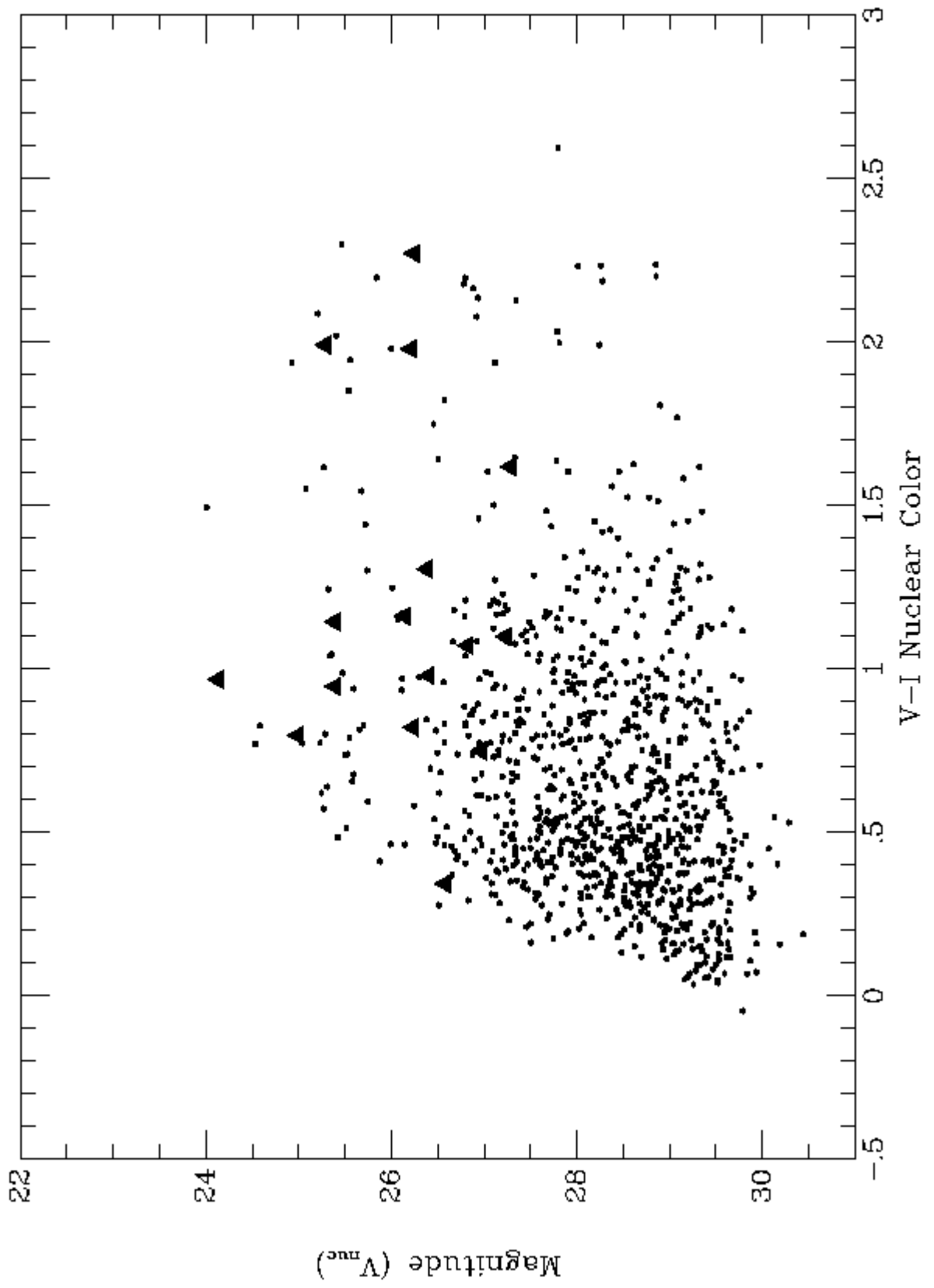


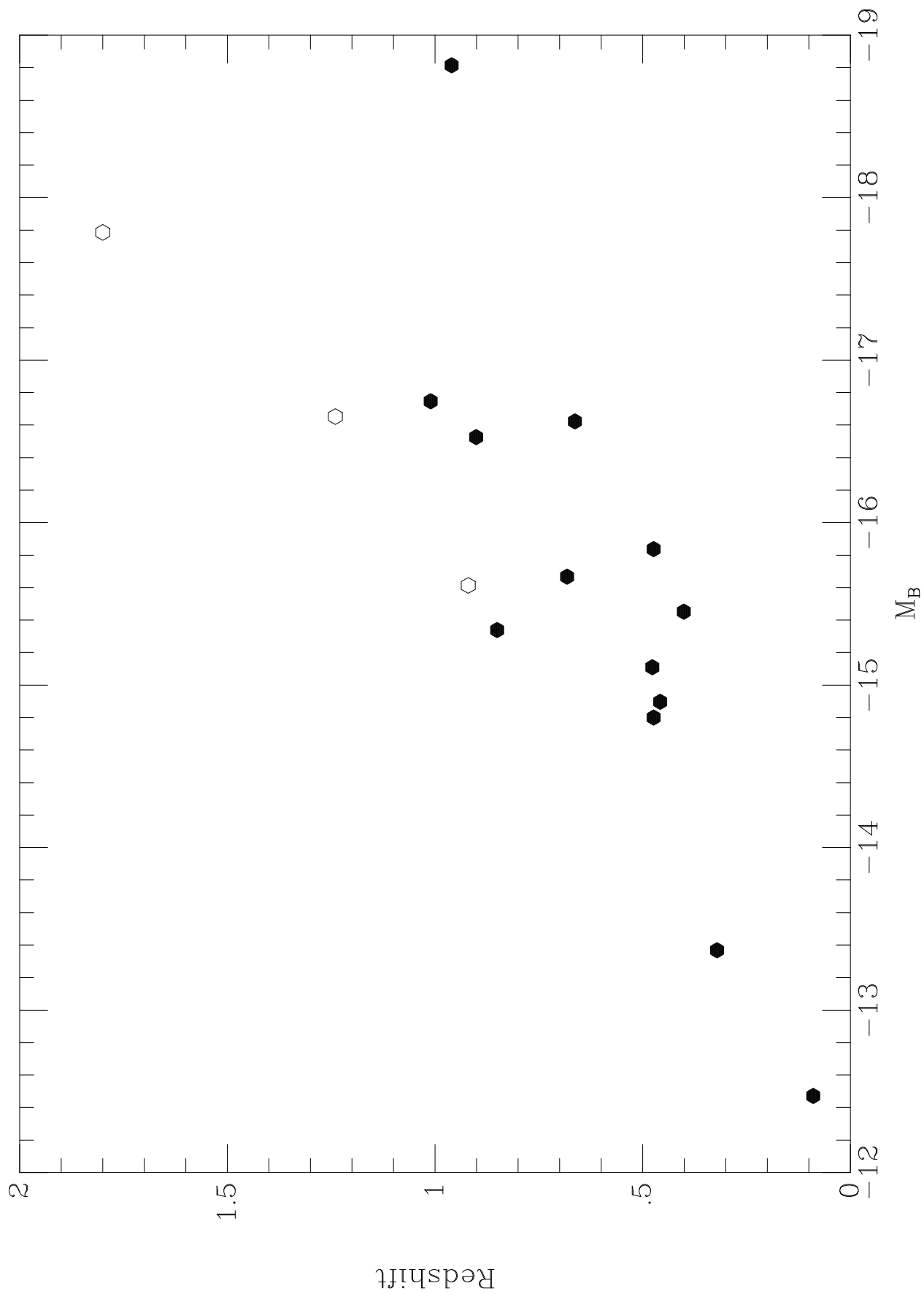












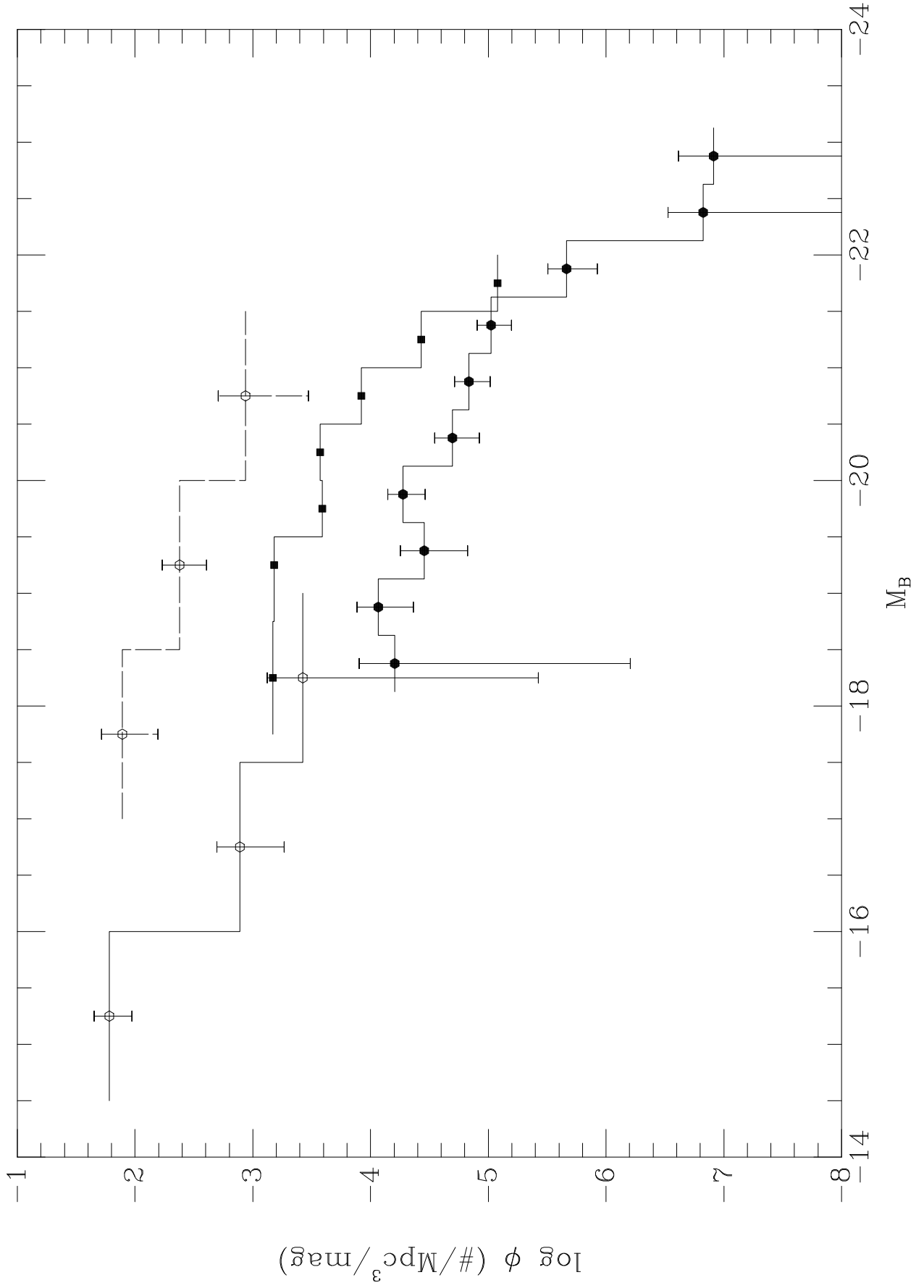


Fig. 1.— Magnitude difference between the 1995 and 2000 images as a function of magnitude within an aperture of $r=3$ pixels ($0.15''$ diameter). The solid line represents no difference in magnitude between the two epochs.

Fig. 2.— CTE-corrected magnitude difference (1995–2000).

Fig. 3.— a) The magnitude difference for galaxies measured in the odd and even data sets (see text) vs. the average magnitude within $r=3$ pixel apertures. b) The RMS of the magnitude differences in unity magnitude bins. The solid line represents a quadratic fit to the points.

Fig. 4.— a) Absolute value, CTE-corrected magnitude difference for each source in the HDF. The solid line is the 3σ limit indicating significant variables ($3\times$ the solid line in Figure 3b). Sources above this line are marked with open hexagons. Filled symbols indicate the positions of Chandra X-ray sources from the 2Ms survey (triangles are the 16 main catalog sources and squares are the 2 sources from the supplementary catalog). b) The magnitude differences normalized by the expected photometric error. The Y-axis indicates the level of significance of each source in units of σ . Hexagons and triangles are the same as in a).

Fig. 5.— Sigma distribution for galaxies in the HDF. The X-axis is the absolute value of the normalized magnitude difference (σ) and Y-axis is the natural logarithm of the number of points in 0.25 mag bins. Errorbars represent the poisson statistical errors. Filled circles represent the 719 sources brighter than $V_{nuc}=29.0$ and open squares are the 217 sources brighter than $V_{nuc}=27.5$. The curved lines are gaussian fits to the data within 2.5σ ; the solid line is the fit to data brighter than $V_{nuc}=29.0$ and the dashed line is the fit to data brighter than 27.5.

Fig. 6.— V-band images of the 16 galaxies with variable nuclei. Images are $3''$ square and scaled to the same maximum pixel value.

Fig. 7.— V–I Color magnitude diagram of the galaxy nuclei in the HDF. Filled triangles indicate the variable nuclei.

Fig. 8.— Absolute magnitudes of the variable nuclei vs. redshift. Filled circles are spectroscopic redshifts; open circles are redshifts determined indirectly (see Table 1)

Fig. 9.— The luminosity function for variable nuclei in the HDF at $0.4 < z < 1.1$ (open circles) at $\langle z \rangle = 0.69$. The local Seyfert luminosity functions of Huchra & Burg (1992; filled circles) from the CfA survey and Ulvestad & Ho (2001; filled squares) from the Palomar survey are shown. The dashed LF represents the HDF variables if the total galaxy light is included in the absolute magnitude.

Table 1. Variable Nuclei in the HDF

ID ^a	RA (12:36)	DEC (+62)	Redshift	Type ^b	B/T ^c	V_{nuc}	Δ_{nuc}	σ	X-ray ID ^d	offset	MIR ID ^e	offset	Radio ID ^f	offset
2-860.0	54.102	13:54.35	0.851 ^g	3	0.00 (1.25)	27.293	0.107	3.53	HDF-PM3-34	2.650
2-456.22	50.027	13:51.99	1.8 ^h	...	0.52 (1.08)	26.587	-0.056	3.23
2-251.0	46.344	14:04.62	0.960 ⁱ	2	1.00 (1.76)	24.134	0.097	6.48	171	0.194	HDF-PM3-20	1.439	192	0.048
3-355.0	56.923	13:01.56	0.474 ^j	2	0.94 (1.00)	26.388	-0.048	3.20	203	0.066	HDF-PS2-4	2.116	225	0.604
3-863.0	58.649	12:21.72	0.682 ^l	4	0.00 (1.14)	26.411	0.046	3.06
3-943.0	56.432	12:09.31	0.321 ^l	3	0.00 (1.23)	26.972	0.095	4.04	224	2.074
3-143.0	49.644	12:57.43	0.477 ^l	2	0.00 (1.58)	26.148	0.070	4.65
3-659.1	51.722	12:20.18	0.401 ^j	2	0.00 (1.50)	25.390	0.060	4.02	190	1.235	HDF-PM3-29	1.501	209	1.155
3-386.111	50.254	12:39.72	0.474 ^l	3	0.00 (6.23)	25.397	0.057	3.77	HDF-PS3-16	0.823
3-777.1	52.022	12:09.63	0.458 ^g	4	0.53 (1.14)	26.24	0.048	3.21
3-965.111111	57.485	12:10.55	0.663 ^g	1	...	25.293	-0.141	9.42	206	0.456
4-254.0	46.127	12:46.50	0.901 ^g	1	0.90 (1.03)	26.216	-0.049	3.28	HDF-PS3-17	2.182
4-516.0	45.652	11:53.97	1.24 ^m	3	0.66 (1.08)	26.827	-0.074	3.54
4-752.1	44.377	11:33.20	1.011 ^j	1	0.87 (1.25)	26.250	-0.046	3.07	165	0.210	187	0.121
4-801.0	39.990	12:33.65	0.920 ^k	4	0.17 (1.07)	27.234	0.096	3.33
4-976.1	41.643	11:31.85	0.089 ^l	4	0.00 (19.1)	24.998	0.054	3.60	160	1.112	HDF-PM3-12	3.308

^aGalaxy ID from Williams *et al.* 1996.

^bSpectroscopic type based on photometry from FLY: 1=E/S0, 2=Sbc, 3=Scd, 4=Irr

^cBulge fraction from Marleau & Simard (1998) followed by the chi-square goodness of fit in parantheses.

^dX-ray ID number from in Brandt *et al.* (2001).

^e15 μ m ID from in Aussel *et al.* (1999).

^f1.4GHz ID number from in Richards *et al.* (1999).

^gRedshift from Cohen *et al.* (2000).

^hFLY does not provide a photometric redshift for this source. The authors have estimated the redshift based on the photo-z's of other galaxies having similar colors in the FLY catalog.

ⁱRedshift from Phillips *et al.* (1997).

^jRedshift from Barger *et al.* (2002).

^kRedshift Photometric redshift from FLY.

^lRedshift from Cohen *et al.* (1996).

^mRedshift based on absorption feature observed in a nearby galaxy spectrum (Bunker *et al.* 2000)